Knot Fingerprints Resolve Knot Complexity and Knotting Pathways in Tight Knots

David A B Hyde & Kenneth C Millett *
Joshua Henrich & Eric J Rawdon †
Andrzej Stasiak ‡

April 29, 2013

Abstract

Knot fingerprints provide a fine-grained resolution of the local knotting structure of tight knots. From this fine structure and an analysis of the associated planar graph, one can define a measure of knot complexity using the number of independent unknotting pathways from the global knot type to the short arc unknot. A specialization of the Cheeger constant provides a measure of constraint on these independent unknotting pathways. Furthermore, the structure of the knot fingerprint supports a comparison of the tight knot pathways to the unconstrained unknotting pathways of comparable length.

1 Introduction

Within the natural sciences, knotted, linked, or entangled macromolecules are encountered in a wide range of contexts and scales. Their presence has important implications for physical and biological properties. Understanding how their presence causes these observed properties is a matter of contemporary interest. In this research, we focus on the local structure of a robust family of knots, the ideal knots [49]. Our focus identifies the locus of the constituent local knots of a knotted ring, as expressed in the knotting fingerprint, and their interrelationship [43, 44]. To identify the fine-grain knotting structure of a complex knotted ring, we employ the MDS method [25, 26] that defines the knot type of each subchain of the ring. We display this information in the form of a color-coded disc in which the color corresponds to the identified knot type. The radial distance from the center expresses the length of the subchain, with short subchains near the center and the entire chain giving the border of the

*Department of Mathematics,University of California, Santa Barbara, CA 93106, USA
†Department of Mathematics, University of St. Thomas, St. Paul, MN 55105, USA
‡Center for Integrative Genomics, University of Lausanne, CH-1015 Lausanne-Dorigny, Switzerland

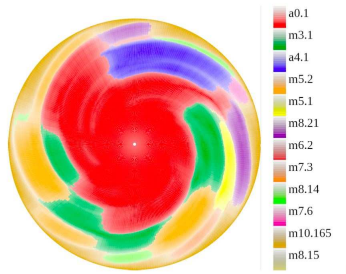

Figure 1: The knotting fingerprint of 10_{165}

disc. The angular coordinate expresses the starting point of the subchain such as shown in Figure 1. This knotting fingerprint is then translated into the planar graph associated to the fingerprint. The vertices in this graph correspond to the associated knot type regions. Among these vertices, the central unknot (as short segments are never knotted) and the peripheral region corresponding to the global knot type have special roles. We assess the complexity of the knot by looking at a measure of constriction inspired by the Cheeger Constant. We also look at a measure of structural complexity using the number of edge- and vertex-independent paths in the graph that begin at the central unknot vertex and end at the global knot vertex. These measures provide information associated with the spatial properties of the knot. For example, the number of independent paths is precisely the number of independent unknotting/knotting pathways associated to the given spatial conformation. Further analysis suggests ways that are three-dimensional in character by which one can measure the spatial complexity of the knot, in contrast to the classical measure associated to minimal crossing knot projections.

2 Ideal Knots

Ideal knots [49] are inspired by the result of tying a knot in some physical material (e.g. a piece of rope of some uniform thickness) and then seeking a conformation of the knot in which the length is the smallest possible. Thus, in the context of this study, we consider circular ropes of uniform thickness and minimal length among all conformations representing the same knot type. Such conformations are mathematically modeled by smooth curves, usually $C^{1,1}$ or C^2, for which one can define the radius of an embedded normal tube and the length of the curve. The *ropelength* of a knot is defined to be the minimum of ratios of this radius and the length over all conformations of a given knot type. A curve realizing this minimum is then a *tight knot* or, equivalently, an *ideal knot*. Rigorous results for tight knot conformations are very limited. For example, we only have estimates of the minimal ropelength for the trefoil knot, i.e. it lies between 31.32 and 32.74317 [40, 41]. As a consequence, we are limited to approximate conformations described by polygons resulting from computer simulations. In this research, we apply our analysis to the ideal prime knot and composite knot conformations resulting from the knot-tightening code *ridgerunner*, developed by Ashton, Cantarella, Piatek and, Rawdon [38, 42].

3 Knotting Fingerprints

A closed chain in Euclidean 3-space is knotted if there is no ambient deformation of space taking the chain to the standard planar circle. The search for computationally efficient and effective methods to determine the specific structure of knotting for polygons is a continuing mathematical challenge. More importantly, the search for an appropriate formulation of knotting of open chains is even more challenging. From the classical topological perspective, knotting of open polygons is an artifact of a fixed spatial conformation because, if edge lengths and directions in the polygon are allowed to vary, each open polygon is ambient isotopic to a standard interval in the "x"-axis in 3-space (this is popularly called the "light-bulb" theorem). However, open polygons are geometrically knotted if the edge lengths are fixed. This is demonstrated by the examples of Canteralla-Johnson and others [27, 28, 29]. If one considers the case of equilateral polygons, it is unknown at this time whether or not there are configurations that cannot be deformed to a straight segment preserving the edge lengths. The analogous problem for closed equilateral polygons is also unknown, i.e. "Are there topologically unknotted equilateral polygon configurations in 3-space that cannot be deformed to the standard planar equilateral polygon?" These two problems give one a sense that the degree of difficulty in describing the knot theory of equilateral polygons in 3-space is considerable. Beyond those equilateral polygons having 8 or fewer edges, for which one knows more [30, 31, 32], one does not even know how many topological knot types can be achieved. If one adds thickness to the structure, one faces the Gordian Knot, which can only be unknotted by making it longer or thinner [45, 46]. While we focus here on prime knots and simple composite knots, one expects that Gordian Knots, whose cores are topologically unknotted, will also exhibit important complexity in their knotting fingerprint.

In this study of knots, it is important to be sensitive to questions of chirality, i.e. the spatial orientation of the knot in 3-space. A knot is said to be *chiral* if it is not equivalent to its mirror reflection. For many chiral knots, the *writhe* of a minimal crossing projection (defined as the algebraic sum of the crossing numbers, see Figure 2) is not zero, thereby defining a positive/negative instance dependent upon whether the writhe is positive/negative. If the specific knot, K, has positive writhe, it may be denoted by K, by +K, or by pK, depending upon the setting. If the negative instance is selected, it will always be denoted by -K or mK. Achiral knots, i.e. those equivalent to their mirror reflections, will have 0 writhe; however, this condition is not sufficient to determine whether or not the knot is achiral, as there are chiral knots having minimum crossing presentations of 0 writhe.

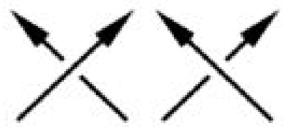

Figure 2: +1 and −1 algebraic crossing numbers

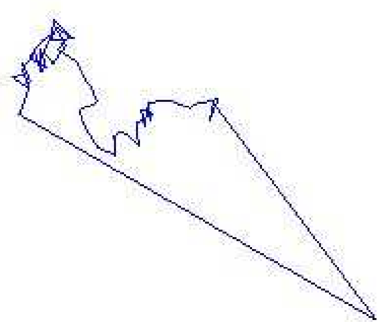

Figure 3: The *MDS* knotting closure

3.1 The *MDS Method*

In order to identify the knotting present in open chains, especially those used as models for protein structures, and being concerned with the uncertain features of some popular strategies, Millett, Dobay and Stasiak [25, 26] developed a stochastic method to identify and quantitatively measure the extent of knotting present in an open polygonal segment. This method was employed in a study of knotting in random walks and tested against the previously identified knotting present in protein structures. More recently, it has been employed to create the knotting fingerprint used in an extensive study of the presence and nature of knots and slipknots occurring in protein structures [43]. The *MDS Method* is described as follows: given an open polygonal arc, consider the distribution of knot types, the *knotting spectrum* (see Figure 4), arising from the connection of both endpoints of the polygon to a uniform distribution of points on the sphere of very large radius that plays the role of the "sphere at infinity" (see Figure 3). For all practical purposes, this spectrum identifies a dominant knot type at the plurality level. Thus when a single knot type occurs more than any other knot type in the closures, we identify this as the knot type of the segment and record the proportion of this knot type. In a test of one thousand 300-step random walks in 3-space, the 0.50 level test was successful 99.6% of the time [25]. As a consequence, the MDS approach provides a powerful method with which to analyze the knotting of open chains.

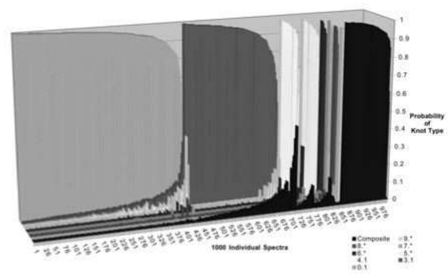

Figure 4: The *MDS* knotting spectrum of $1,000$ 300-step random walk

3.2 The Knotting Fingerprint

For a given knotted or unknotted polygonal ring of n segments, one constructs the *knotting fingerprint* by first determining the knotting spectrum for each subsegment of the chain. The color is determined by the predominant knot type, and the intensity of the color is determined by the proportion of *MDS* closures having the given knot type. These colored cells are arranged as follows. First, a base point and orientation of the chain is selected. For a given segment length, starting at one and increasing to n, the colored segments are arranged at a constant radius corresponding to the proportion of the total length of the chain in a counter-clockwise fashion, with the angle indicating the proportion of the circuit from the base point to the start of the segment in the direction of the orientation. In Figure 5, we show the knotting fingerprint of an ideal 9_2 knot. The color bar in the right of the figure indicates the color code and intensity range for this knotting fingerprint. The color of the unknot is indicated by the color red. As very short segments of three or shorter must be unknotted, the central region of the knotting fingerprint is always red. As the entire chain is always the global knot type, the outer ring of the knotting fingerprint is the color attributed to the knot type. Each of the colored regions provides information about the knotting structure of the chain. For example, reading the color coding of rings of increasing radius, i.e. proportion of the total circular chain, one can estimate the length of the shortest subsegment supporting the global knot type.

3.3 Analysis of the Knotting Fingerprint

The knotting fingerprints may be limited by resolution of the knot type they represent, i.e. corresponding to the number of segments in the chain. Hence there are certain scenarios where the apparent knotting fingerprints do not agree with what we would expect. In some cases, this is a matter of resolution while, in others, it may give evidence of an unanticipated evolution of the local structure. For example, we frequently observe tiny, e.g. single cell, isolated regions of a certain type near but not contiguous to much larger regions of the same type. When this phenomenon occurs near the boundary of two regions in the knotting

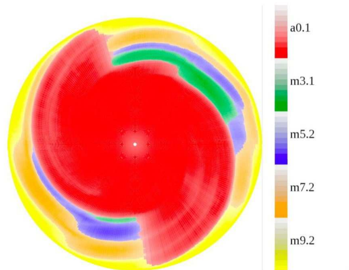

Figure 5: The knotting fingerprint of an ideal 9_2

fingerprint, it suggests that the tiny regions are inadvertent artifacts, due to the limited resolution, and should not be considered as singular regions distinct from their larger neighbors of the same type. In such situations it may be appropriate to "smooth" the data so the boundaries between distinct regions are more regular.

In other situations, we observe features in the knotting fingerprint that appear to be inconsistent with one's interpretation of the consequences of knot theory. For example, there are several cases when the global knot has an unknotting number greater than one, but the unknot appears to connect to the global knot by the addition of a single segment. One might expect that the difference between unknotting numbers of adjacent regions must be no greater than one [48, 47], so these fingerprints appear to be incorrect. For a single closure point on the sphere, the addition of a sufficiently small edge would account for no more than a single strand passage, but in our case, there are two features that weaker this simplistic analysis. First, for a single closure point, our edge addition may cause more than one strand passage. This situation could be eliminated through a higher resolution, i.e. subdivision of the edge segments of the chain. Second, our analysis concerns a stochastic process giving spherical regions representing the distinct knot types arising from the closures. The process of adding an edge causes an evolution of these regions. Thus our choice of the plurality knot type can lead to a jump of two or more in the strand passage difference between the competing knot types (see Figure 6). We will see this represents a real artifact of the ideal knot presentation, not merely a question of its resolution. Therefore, although with greater resolution we would see a more accurate knotting fingerprint, the strand passage difference between two adjacent regions may or may not reflect the real structure of the ideal knot. For these analyses, one can carefully account for this potential error by deleting the edge between the unknot and the global knot in the corresponding knotting graph when the idea knot structure suggests that is a resolution artifact.

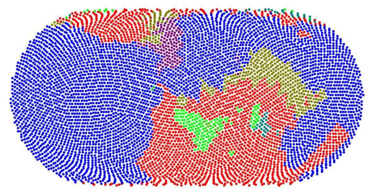

Figure 6: Eckert IV prevention of the spherical distribution of knot types

3.4 The Knotting Graph

The knotting fingerprint defines the planar *Knotting Graph* by associating a vertex for each of the knotting regions, the connected components of the knotting fingerprint, and edges connecting vertices corresponding to contiguous regions. In Figure 7, we show the Knotting Graph associated to the 9_2 graph. The addition of this edge corresponds to the movement of one of the edges connecting to the sphere during which one may pass through one or more other edges of the associated conformation. If the resolution of the ideal knot is fine enough, one would expect that a single passage would occur and the unknotting numbers of the associated closed conformations could change by at most one. The designation of the knot type being given to that type attaining the plurality makes our analysis of the knotting fingerprint and the associated graph even more complex. The phenomenon that addition of a single small segment can correspond to a jumping unknotting number of two or more is quite possible and actually occurs. Thus one needs to look very closely at the possibility of a complex structural evolution (see Figure 11).

The knotting graph has two distinguished vertices. The first corresponds to the component of small unknotted segments, labeled $a0.1$. The second corresponds to the knot type of the entire ring, labeled $m9.2$ in Figure 7, indicating that it is the "minus 9_2" knot according to the classical knot enumeration. In addition, there are two components of $m3.1$, $m5.2$, and of $m7.2$ shown in Figure 5, each giving a vertex in the knotting graph in Figure 7. There are edges between the $m3.1$ vertices and the 0.1 and 5.1 vertices, as the green 3.1 component shares common frontiers with the red 0.1 and blue 5.1 components.

4 Analysis of the Knotting Graph

In this paper we employ the knotting graph associated to the knotting fingerprint of a given knot as the principal vehicle supporting our analysis of the complexity and character of the knot. The unknot vertex and the global knot vertex anchor our analysis as we study the extent to which there are constraints inherent in the evolution from the unknot to the global knot reflected in the structure of the knot. For example, to what extent is this evolution constrained? Are there a small number of knotting states through which this evolution must pass? One powerful measure of such a constraint or "bottleneck" is provided

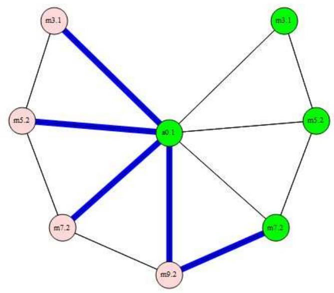

Figure 7: The knotting graph of an ideal 9_2

by a specialization of the Cheeger Constant.

4.1 The Cheeger Constant

In graph theory, the *Cheeger Constant* is a measure of whether a graph contains a "constriction" or "bottleneck." It is inspired by Cheeger's isoperimetric constant $h(M)$ for a compact Riemannian manifold, M, in terms of the area of a codimension one hypersurface, S, dividing the manifold into two disjoint pieces of equal volume. For graphs, the Cheeger Constant is defined as follows: Let G denote a connected graph, $V(G)$ be the vertices of G, and $E(G)$ be the edges of G. For a subset of vertices, S, containing either the initial unknot vertex or the global knot vertex (but not both), let ∂S denote the set of edges that has exactly one vertex in S and let $|\partial S|$ be the number of such edges. We define the *Cheeger Constant* by

$$h(G) = minimum \left\{ \frac{|\partial S|}{|S|} \mid 0 < |S| \leq \frac{|V(G)|}{2} \right\}$$

This formulation of a Cheeger Constant is designed to detect the presence of a constriction in the separation of the knotting graph that lies between the trivial knot and the global knot and, as such, represents a constriction in the growth of the knotting structure. In Figure 7, we show the set of vertices, $S = \{0.1, m3.1, m5.2, m7.2\}$, connected by five edges to the remaining vertices, including the global knot vertex. This configuration gives the minimal Cheeger Constant equal to $\frac{5}{4}$ which, since it is greater than one, indicates that the 9_2 knotting fingerprint does not suggest a constriction in its knotting.

4.2 Independent Knotting Pathways

Another possible measure of constriction is inspired by the *Max-Flow-Min-Cut* Theorem and the related theory of Menger. We determine the maximum number of edge independent paths, i.e. no edge appears in more than one path, from the unknot vertex to the global knot vertex. In Figure 7, we observe that the

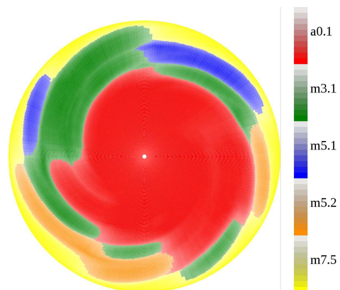

Figure 8: The 7_5 knot illustrates the difference between $ER(K) = 6$ and $EVR(K) = 5$

maximum number of edge independent paths from the unknot vertex to the global knot vertex is 3 as, in this case, the constraint is given by the degree of the global knot vertex. An initial analysis shows that the maximal number of edge independent paths is bounded above by the degree of the unknot vertex, the degree of the global knot vertex, and the number of edges in the minimum edge cut set separating the unknot vertex from the global knot vertex. The number of edges in the minimum edge cut set is related to the Cheeger Constant as well as the Max-Flow analysis. We propose to call the maximum number of edge independent paths the *edge robustness index*, $ER(K)$, of the knotting graph.

We observe, as is shown in Figure 7, that the specific set of paths in not unique.

Perhaps it is more appropriate to require that the connecting paths are both edge and vertex independent. In this case one defines the *edge vertex robustness index*, $EVR(K)$, of the knotting graphs. We note that there are cases in which these two indices of a knotting graph are different. The smallest crossing number example is the knot 7_5, whose knotting fingerprint is shown in Figure 8. An analysis of the associated knotting graph, Figure 8, shows that there are 6 edge independent paths while there are only 5 edge-vertex independent paths.

4.3 Second Order Pathway Independence

In an analysis of knotting graphs, one discovers a collection of knots for which the $EVR(K)$ is equal to 1 due to the existence of a *bridge edge* in the graph, i.e. an edge whose removal disconnects the unknot vertex from the global knot vertex. The simplest examples of this structure are the $(2, n)$-torus knots, see Figure 9. In this case, this is the dominant theme, i.e. all edges are bridges. In other cases, this first measure of robustness may not fully capture the complexity of the knotting fingerprint. One is lead, as a consequence, to create a second order measurement associated to the two connected components that result from the removal of the bridge edge. One of the bridge's vertices can be identified as a terminal vertex when it lies in the component containing the unknot vertex, while the other can be identified as an initial vertex of the other component. We

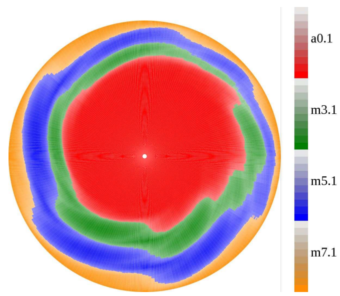

Figure 9: The 7_1 torus knot has a linear knotting graph

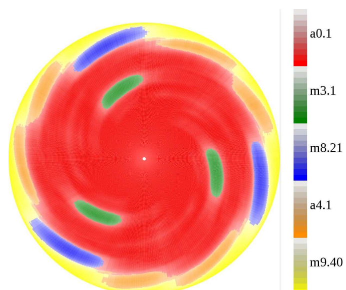

Figure 10: The 9_{40} knot

then determine the edge vertex robustness index for the two resulting subgraphs, thereby giving a pair of indices, (p, q), that define the second level of pathway independence. In some cases, the bridge is adjacent to the unknot vertex or the global knot vertex. In such cases, we assign the index 0 to the component consisting of the single vertex.

4.4 Prime, Composite, and Slipknots in Knotting Fingerprints

We have seen that the knotting fingerprints of ideal prime knots can be quite complex (see Figure 1), in that there can be a complex spectrum of knot types found among its substructures. One may find subknots of a prime knot that are slipknots, i.e. they are contained with larger segments which are unknotted (see Figure 10). Ideal composite knots, the connected sums of two or more prime knots, exhibit even more complex structure (see Figure 11). Despite having two distinct 3_1 knot components, the knot graph of $3_1\#3_1$ is linear corresponding to 3_1. In contrast, $-3_1\#3_1$ exhibits two distinct components for the summands separated by an unknot region. In this knot graph, the unknot component is contiguous to the connected sum component, a knot of unknotting number two. Thus, the fine structure of the knotting evolution in this area must be much more complex, perhaps along the lines discussed earlier, in which there is an evolving

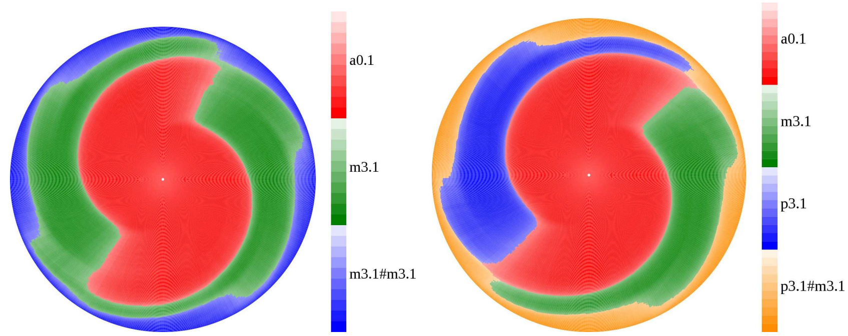

Figure 11: The knotting fingerprint of connected sums: $3_1\#3_1$ and $-3_1\#3_1$

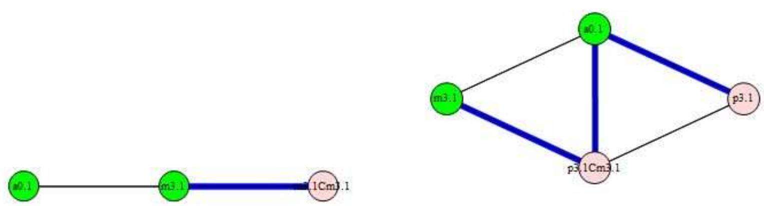

Figure 12: The knotting graph of connected sums: $3_1\#3_1$ and $-3_1\#3_1$

proportion that includes the unknot and the two distinct summands. In the case where the two summands are the same type, their knot type is cumulative, thereby providing the ring separation observed in the knotting fingerprint.

5 Knot Complexity

In the following tables, we present our determinations of these measures of knot complexity.

5.1 Cheeger Constant Complexity

With sufficient resolution, one observes that the only n-vertex linear knotting graphs observed are associated with the family of $(2, 2n+1)$-torus knots, for which the Cheeger constant is $\frac{1}{n}$, the smallest values observed. In our data, this is the case for $3_1, 5_1$, and 7_1. For 9_1, we see that this is no longer the case, though one can easily see that it should also be confirmed with a finer resolution (see Figure 13). One expects to see complete rings of each knot type, as in the case of 7_1 (see Figure 9), but here the 5_1 and 7_1 rings are incomplete due the lack of sufficient resolution.

This phenomenon is quite different from the one observed most clearly in the case of the connected sums of trefoil knots. There are two chirally distinct

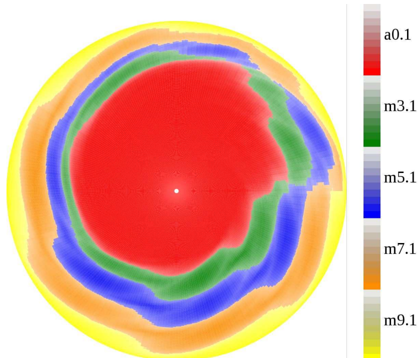

Figure 13: Ideal 9_1

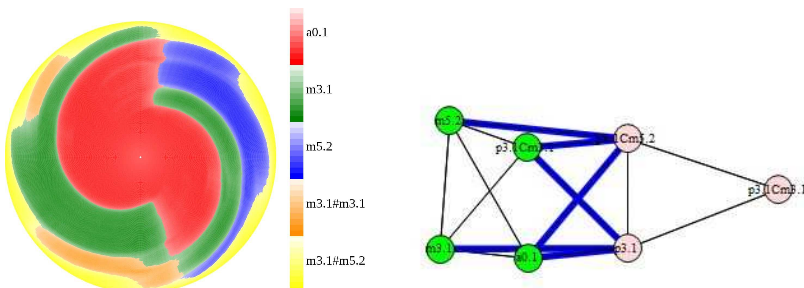

Figure 14: Ideal $3_1\#5_2$ knotting fingerprint and associated knotting graph

cases depending upon the the writhe, i.e. the algebraic sum of the crossings numbers: the left trefoil, denoted -3_1, has negative writhe and the right trefoil, denoted 3_1 has positive writhe. In Figure 12, one sees that $3_1\#3_1$ has a linear graph, as its knotting fingerprint consists of concentric rings similar to the torus knot case. The graph of -$3_1\#3_1$ is more complex because the unknot region and the global knot region are contiguous. As mentioned earlier, this contiguity is associated with the interplay between the two types of trefoils that prevent their knotting regions from contiguity and, thereby, forcing the surprising connection between the unknot and the connected sum, an unknotting number two knot. An even more complex example of this phenomenon is exhibited by the knotting fingerprint of the connected sum, $3_1\#5_2$ and the associated knotting graph (see Figure 14).

As measured by the Cheeger constant, the most complex knotting fingerprints among those in our current tables are 8_3 and 9_{44} whose knotting graphs are shown in Figure 15.

5.2 Independent Path Complexity

Since the numerator of the Cheeger constant is the number of edges in an edge-cut set separating the global knot from the unknot, this numerator gives an upper bound on the number of edge independent paths connecting the unknot region to the global knot region. From the tables, one sees that EVR is often a bit smaller than this numerator. Such is the case for the knot 7_2 in Table 1. If one employs EVR(K) as a measure of complexity instead of the Cheeger constant, one finds that the $(2, n)$-torus knots are identified as the simplest structures, along with 8_{14}, 8_{19}, and 9_{35}. The most complex, having 14 independent pathways, are 9_{29}, 9_{32} and 9_{33}. These latte knots suggest that the independent pathway measure may capture a distinctly new dimension of knot complexity.

While there is only one minimal path taking the trefoil knot 3_1 to the unknot 0_1, the story is more complex for other $(2, n)$-torus knots. For 5_1, an unknotting number two knot, the shortest paths must have length two. However, these paths are no longer unique, as one may add any single strand passage resulting in an unknotting number one knot, creating another shortest path. Employing "TopoIce-X" within the KnotPlot software [50], we find that in addition to $5_1 \to 3_1 \to 0_1$, one must also consider $5_1 \to 5_2 \to 0_1$, $5_1 \to 8_7 \to 0_1$, and $5_1 \to 9_{26} \to 0_1$, staying within the class of knots of crossing number no larger than 10. In the knotting fingerprint for 5_1, only the first unknotting pathway is observed. For 7_1, the situation is much more complex. In addition to the $7_1 \to 5_1 \to 3_1 \to 0_1$ pathway, the three other previous pathways occur. Adding even more pathways are those knots starting with $7_1 \to 7_3$, $7_1 \to 7_5$, and $7_1 \to 10_5$ since each of these is an unknotting number two knot with their own selection of unknotting pathways. Again, only the first occurs for the ideal 7_1. The constraint that the knotting pathway be supported by knotted subsegments of the ideal knot effectively limits the knotting pathway options to the "standard $(2, n)$-torus knot" pathway, despite the knot graph complexity whose occurrence we associate with the need for greater resolution (larger number of edges) to capture essential features of the structure.

The twist knots provide another interesting class to consider, the first of which is 5_2, an unknotting number one knot. Thus, its shortest path is $5_2 \to 0_1$ but, as 3_1 is a subknot of 5_2 there is a second, independent unknotting pathway $5_2 \to 3_1 \to 0_1$ within its knotting fingerprint. Furthermore, there are two disjoint 3_1 components giving rise to a second, independent $5_2 \to 3_1 \to 0_1$ unknotting pathway. As a consequence, both the Cheeger constant, 1.50, and EVR, 3, provide a better measure of the real structural complexity of the twist knot. This same complex structure is exhibited in the knotting fingerprints of 6_1, 7_2, 8_1, and 9_2.

What does this tell us about more complex knots, e.g. 8_3 shown in Figure 15? The Cheeger constant is 2.00 and EVR is 8. It is an unknotting number two knot whose knotting fingerprint contains $\pm 6_1$ and 4_1 supporting knotting pathways: $8_3 \to -6_1 \to 0_1$, $8_3 \to -6_1 \to 4_1 \to 0_1$, $8_3 \to +6_1 \to 0_1$, and $8_3 \to +6_1 \to 4_1 \to 0_1$. Due to a two-fold symmetry, there are actually two

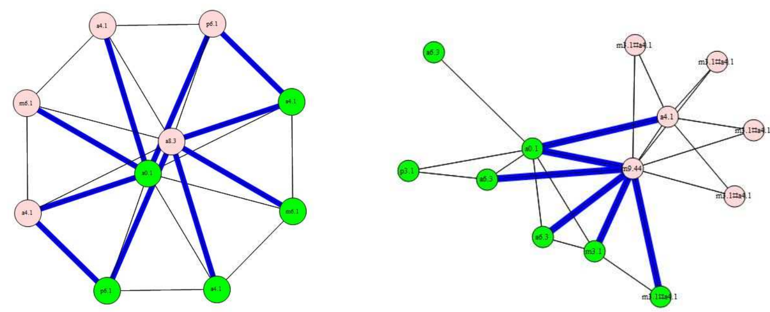

Figure 15: h(8_3) = 2.00 and h(9_{44}) = 1.86

examples of each of these knotting pathways, resulting in a total of 8, the EVR.

Another complex knot is 9_{44} (see Figure 15), an unknotting number one knot whose Cheeger constant is 1.86 and EVR is 7. As 9_{44} is not a rational knot, TopoICE does not list the knot, but we know that it has unknotting number one, giving the minimal path. There are, however, seven independent paths, again providing a substantial measure of complexity. We note that 9_{44} contains a composite sub knot, $-3_1\#4_1$, that has unknotting number two.

6 Conclusions

In this paper we have presented the knotting fingerprint of a polygonal approximation of an ideal knot, or tight knot, showing the structure of the knotting of subsegments of the knot. The associated subknot types define regions of the knotting fingerprint, i.e. a planar map, to which one can associate a planar graph with two distinguished vertices corresponding to the unknot and the global knot. We propose that the complexity of the knotting fingerprint and the associated knotting graph provides a measure of the intrinsic complexity of the knot. Interested in the ways in which knots can be unknotted or, inversely, constructed from unknotted segments, we have proposed two strategies by which one can quantitatively measure this complexity. The first strategy is analogous to the Cheeger constant, h(K), of the graph whereby we partition the vertices of the graph (requiring the unknot to be a member of one subset and the global knot to be a member of the other subset) and take the minimum ratio of the number of edges connecting the two subsets and the number of vertices in the small subset over all such partitions. The second method, EVR(K), is defined to be the number of edge and vertex independent paths in the graph connecting the unknot vertex to the global knot vertex.

Our analysis of prime knots through 9 crossings and a sampling of 10 crossing knots and composite knots demonstrates that these measures are effective tools for assessing the complexity of an ideal knot. The analysis further identifies

Table 1: Analysis of Ideal Prime Knots (through 7 Crossings)

Knot	$h(K)$	$ER(K)$	$EVR(K)$
3_1	$\frac{1}{1} = 1.00$	1	1
4_1	$\frac{1}{1} = 1.00$	1	1
5_1	$\frac{1}{2} = 0.50$	1	1
5_2	$\frac{3}{2} = 1.50$	3	3
6_1	$\frac{3}{2} = 1.50$	3	3
6_2	$\frac{5}{3} = 1.67$	5	5
6_3	$\frac{5}{3} = 1.67$	5	5
7_1	$\frac{1}{3} = 0.33$	1	1
7_2	$\frac{4}{3} = 1.33$	3	3
7_3	$\frac{8}{5} = 1.60$	6	6
7_4	$\frac{7}{4} = 1.75$	4	4
7_5	$\frac{6}{5} = 1.20$	6	5
7_6	$\frac{7}{4} = 1.75$	7	7
7_7	$\frac{7}{5} = 1.40$	7	7

Table 2: Analysis of Ideal Knots (8 Crossing Knots)

Knot	$h(K)$	$ER(K)$	$EVR(K)$
8_1	$\frac{4}{3} = 1.33$	3	3
8_2	$\frac{8}{5} = 1.60$	7	5
8_3	$\frac{10}{5} = 2.00$	8	8
8_4	$\frac{11}{6} = 1.83$	9	9
8_5	$\frac{8}{5} = 1.60$	6	4
8_6	$\frac{9}{6} = 1.50$	8	8
8_7	$\frac{8}{6} = 1.33$	7	5
8_8	$\frac{11}{6} = 1.83$	10	10
8_9	$\frac{11}{7} = 1.57$	10	9
8_{10}	$\frac{10}{6} = 1.67$	7	7
8_{11}	$\frac{10}{7} = 1.43$	10	10
8_{12}	$\frac{7}{5} = 1.40$	6	6
8_{13}	$\frac{9}{7} = 1.29$	9	9
8_{14}	$\frac{1}{1} = 1.00$	1	1
8_{15}	$\frac{9}{6} = 1.40$	4	4
8_{16}	$\frac{13}{8} = 1.63$	13	13
8_{17}	$\frac{9}{6} = 1.50$	8	8
8_{18}	$\frac{9}{6} = 1.50$	9	9
8_{19}	$\frac{1}{1} = 1.00$	1	1
8_{20}	$\frac{6}{4} = 1.50$	5	5
8_{21}	$\frac{6}{4} = 1.50$	4	4

Table 3: Analysis of Ideal Knots (9 Crossing Knots)

Knot	$h(K)$	$ER(K)$	$EVR(K)$
9_1	$\frac{1}{1} = 1.00$	1	1
9_2	$\frac{5}{4} = 1.25$	3	3
9_3	$\frac{11}{7} = 1.57$	6	6
9_4	$\frac{10}{8} = 1.25$	8	8
9_5	$\frac{12}{9} = 1.33$	10	10
9_6	$\frac{8}{6} = 1.33$	6	4
9_7	$\frac{11}{7} = 1.57$	7	7
9_8	$\frac{11}{6} = 1.83$	9	9
9_9	$\frac{9}{7} = 1.29$	5	4
9_{10}	$\frac{11}{10} = 1.10$	8	7
9_{11}	$\frac{12}{8} = 1.50$	11	7
9_{12}	$\frac{11}{8} = 1.38$	10	10
9_{13}	$\frac{12}{9} = 1.33$	8	6
9_{14}	$\frac{10}{7} = 1.43$	8	8
9_{15}	$\frac{11}{7} = 1.57$	10	9
9_{16}	$\frac{11}{6} = 1.10$	2	2
9_{17}	$\frac{12}{9} = 1.33$	10	10
9_{18}	$\frac{12}{8} = 1.50$	9	7
9_{19}	$\frac{9}{6} = 1.50$	9	8
9_{20}	$\frac{12}{9} = 1.33$	11	10
9_{21}	$\frac{15}{10} = 1.50$	12	11
9_{22}	$\frac{14}{8} = 1.75$	12	12
9_{23}	$\frac{13}{8} = 1.63$	9	8
9_{24}	$\frac{10}{8} = 1.25$	9	8
9_{25}	$\frac{11}{7} = 1.57$	7	7
9_{26}	$\frac{14}{9} = 1.56$	12	10
9_{27}	$\frac{14}{9} = 1.56$	13	12
9_{28}	$\frac{10}{7} = 1.43$	8	7
9_{29}	$\frac{16}{11} = 1.45$	14	14
9_{30}	$\frac{12}{8} = 1.50$	11	9
9_{31}	$\frac{10}{7} = 1.43$	7	6
9_{32}	$\frac{14}{11} = 1.27$	14	14
9_{33}	$\frac{14}{9} = 1.56$	14	14
9_{34}	$\frac{11}{8} = 1.38$	11	11
9_{35}	$\frac{1}{1} = 1.00$	1	1
9_{36}	$\frac{9}{89} = 1.13$	6	5
9_{37}	$\frac{12}{10} = 1.20$	12	10
9_{38}	$\frac{13}{10} = 1.30$	4	4
9_{39}	$\frac{14}{10} = 1.40$	13	11
9_{40}	$\frac{8}{8} = 1.00$	8	8
9_{41}	$\frac{14}{10} = 1.40$	13	12
9_{42}	$\frac{6}{4} = 1.50$	5	5
9_{43}	$\frac{9}{6} = 1.50$	6	6
9_{44}	$\frac{6}{7} = 01.86$	5	5
9_{45}	$\frac{9}{6} = 1.50$	6	5
9_{46}	$\frac{7}{6} = 1.17$	7	7
9_{47}	$\frac{11}{8} = 1.38$	10	10
9_{48}	$\frac{12}{10} = 1.20$	11	10
9_{49}	$\frac{12}{8} = 1.50$	7	6

Table 4: Analysis of Ideal Knots (Selected 10 Crossing Knots)

Knot	$h(K)$	$ER(K)$	$EVR(K)$
10_3	$\frac{11}{9} = 1.22$	8	7
10_5	$\frac{11}{9} = 1.22$	8	6
10_{10}	$\frac{13}{10} = 1.50$	10	10
10_{11}	$\frac{14}{10} = 1.40$	10	10
10_{20}	$\frac{12}{8} = 1.50$	9	9
10_{35}	$\frac{12}{8} = 1.50$	11	9
10_{36}	$\frac{12}{9} = 1.33$	12	10
10_{58}	$\frac{3}{2} = 1.50$	2	2
10_{60}	$\frac{11}{9} = 1.22$	9	9
10_{70}	$\frac{13}{9} = 1.44$	11	10
10_{76}	$\frac{12}{8} = 1.50$	6	4
10_{125}	$\frac{9}{7} = 1.29$	5	5
10_{126}	$\frac{12}{8} = 1.50$	7	6
10_{127}	$\frac{9}{6} = 1.50$	6	5
10_{128}	$\frac{11}{8} = 1.38$	2	2
10_{130}	$\frac{11}{7} = 1.57$	9	7
10_{131}	$\frac{11}{9} = 1.22$	11	8
10_{134}	$\frac{9}{6} = 1.50$	3	3
10_{135}	$\frac{10}{7} = 1.43$	5	5
10_{137}	$\frac{12}{7} = 1.71$	11	11
10_{140}	$\frac{10}{9} = 1.11$	10	9
10_{141}	$\frac{10}{8} = 1.25$	8	8
10_{146}	$\frac{8}{8} = 1.00$	8	6
10_{147}	$\frac{10}{7} = 1.43$	10	9
10_{151}	$\frac{12}{8} = 1.50$	6	5

Table 5: Analysis of Ideal Knots (Composite Knots)

Knot	$h(K)$	$ER(K)$	$EVR(K)$
$3_1\#3_1$	$\frac{1}{2} = 0.50$	1	1
$3_1\#4_1$	$\frac{3}{2} = 1.50$	2	2
$3_1\#5_1$	$\frac{4}{3} = 1.33$	3	2
$3_1\#5_2$	$\frac{5}{3} = 1.67$	2	2
$3_1\#-3_1$	$\frac{3}{2} = 1.50$	3	3
$3_1\#-5_1$	$\frac{3}{3} = 1.00$	3	2
$3_1\#-5_2$	$\frac{6}{4} = 1.50$	4	4

instances of complex evolutionary structure, such as contiguous knotting regions representing knot types separated by more than one crossing change (as reflected in their unknotting numbers). While the $(2, n)$ torus knots are clearly those of simplest structure, our analysis calls attention to the apparently simple structure of some other knots, e.g. $9_{44}, 8_{14}, 8_{19}$, and 9_{35} from the knots with fewer than 10 crossings. Furthermore, we have provided a small sample of examples that demonstrates that the knotting pathways that arise within ideal knots come from a quite specific set of options when compared with the shortest knotting pathways available, without being constrained to be supported within the ideal knot structure.

7 Acknowledgements

We thank T. Ashton, J. Cantarella, A. Lapointe, M. Piatek, and E. J. Rawdon for providing the tight prime and composite knot coordinates studied in this project.

References

[1] D. W. Sumners and S. G. Whittington, J. Phys. A: Math. Theor.,7,1988,1689

[2] N. Pippenger, Discrete Appl. Math.,25,1989,960

[3] H. Kesten,L J. Mathematical Phys.,4,1963,273

[4] Y. Diao, N. Pippenger and D. W. Sumners, J. Knot Theory Ramifications,3,1994,419

[5] Y. Diao, J. Knot Theory Ramifications,**2**,1995,189

[6] H. L. Frisch and E. Wasserman, J. Am. Chem. Soc.,**18**,1961,3789

[7] M. Delbruck, Proc. Symp.Appl. Am. Math. Soc.,**14**,1962,55

[8] S. F. Edwards, Proc. Phys. Soc.,**91**,1967,513

[9] P. Virnau, Y. Kantor and M. Kardar, J. Am. Chem. Soc.,**127**,2005,15102

[10] S. A. Wasserman and N. R. Cozzarelli, Science,**232**,1986,951

[11] M. Mansfield, Str. Bio.,**1**,1994,213

[12] W. Taylor, Nature,**406**,2000,916

[13] P. Virnau, L. Mirny and M. Kardar, PLOS Comp. Bio.,**2**,2006,e122

[14] E. Orlandini, M. C. Tesi, E. J .Janse van Rensburg and S. G. Whittington, J. Phys. A: Math. Gen.,**31**,1998,5953

[15] J. M. Deutsch, Phys. Rev. E.,**59**,1999,2539

[16] A. Y. Grosberg, Phys. Rev.Lett.,85,2000,3858

[17] A. Dobay, J. Dubochet, K. C. Millett, P.-E. Sottas and A. Stasiak, Proc. Natl. Acad. Sci. U. S. A.,**100**,2003,5611

[18] N. P. King, E. O. Yeates and T. O. Yeates, J. Mol. Bio.,**373**,2007,153

[19] K. C. Millett, J. Knot Theory Ramifications,**19**,2010,601

[20] V. Katritch, W. K. Olson, A. Vologodskii, J. Dubochet and A. Stasiak, Phys. Rev. E.,**61**,2000,5545

[21] B. Marcone, E. Orlandini, A. L. Stella and F. Zonta, J. Phys. A: Math. Gen.,**38**,2005,L15

[22] B. Marcone, E. Orlandini, A. L. Stella and F. Zonta, Phys. Rev. E.,**75**,2007,041105-1

[23] E. Orlandini, A. L. Stella and C. Vandesande, Phys. Biol.,**6**,2009,1

[24] Y. Diao, J. C. Nardo and Y. Sun, J. Knot Theory Ramifications,**10**,2001,597

[25] K. C. Millett, A. Dobay and A. Stasiak, Macromolecules,**38**,2005,601

[26] K. C. Millett and B. Sheldon, Ser. Knots and Everything,**36**,2005,203.

[27] J. Cantarella and H. Johnston, J. Knot Theory Ramifications,8,1998,1027

[28] G. Toussaint, Beiträge Algebra Geom.,**42**,2001,301

[29] G. Aloupis, G. Ewald and G. Toussaint, Beiträge Algebra Geom.,**45**,2004,429

[30] J. A. Calvo and K. C. Millett, Ser. Knots and Everything,**19**,1998,107.

[31] J. A. Calvo, Topology Appl.,**112**,2001,137

[32] J. A. Calvo, J. Knot Theory Ramifications,**10**,2001,245

[33] D. Jungreis, J. Knot Theory Ramifications,**3**,1994,455

[34] B. Gaertner,Miniball: http://www.inf.ethz.ch/personal/gaertner/.

[35] B. Ewing and K. C. Millett, Progress in knot theory and related topics,(1997), 51

[36] J. Hoste, Handbook of knot theory, (2005),209

[37] E. E. Kim and H. W. Wyckoff,J. Mol. Biol.,**218**,1991,449.

[38] T. Ashton, J. Cantarella, M. Piatek, and E. J. Rawdon,Exp. Math., **20**, 2011, 57

[39] F. R. K. Chung,Spectral graph theory, CBMS Regional Conference Series in Mathematics 92,1997, 207 pages

[40] E. Denne, Y. Diao and J. M. Sullivan,Geom. Topol., **10**, 2006, 1

[41] J. Baranska, S. Przbyl and P. Pieranski,Eur. Phys. J. B.,**66**, 2008, 547

[42] J. Cantarella, A. LaPointe and E. J. Rawdon,J. Phys. A: Math. Theor., **45**, 2012, 225202

[43] J.I. Sulkowsak, E.J. Rawdon, K.C. Millett, J.N. Onuchic, A. Stasiak,PNAS USA, **109**, 2012, E1715

[44] E.J. Rawdon, K.C. Millett, J.I. Sulkowska, A. Stasiak, Bio. Chem. Trans., , 2013, pp

[45] P. Pieranski, S. Przybyl, A. Stasiak,Gordian unknots ???

[46] A. Coward, J. Hass, ???

[47] A. Flammini, A. Stasiak,Proc. R. Soc. A **463**, 2007, 569-582

[48] I. Darcy, D.W. Sumners,Knots '96: Proc. Fifth Int. Research Institute of Mathematical Society of Japan, World Scientific, 267-278

[49] A. Stasiak, J. Dubochet, V. Katritch, P. Pieranski,Ideal Knots, Ser. Knots Everything, **19**, 1998, 1-19

[50] R.G. Scharein, KnotPlot http://www.knotplot.com, 2012